International Journal of GEOMATE
(Geotechnique, Construction Materials and Environment)
ISSN: 2186-2982 (P), 2186-2990 (O), Japan
Vol. 31, Issue 144, August, 2026, pp. 141-151; DOI: 10.21660/2026.144.5576

NONLINEAR SETTLEMENT MODELING OF STONE COLUMN REINFORCED SAND FOR RINGWALL FOUNDATIONS BASED ON PLATE LOAD TESTS

Mersianty[1], *Ahmad Rifa'i[1] and Teuku Faisal Fathani[1,2]

[1]Department of Civil and Environmental Engineering, Faculty of Engineering, Gadjah Mada University, Indonesia; [2]Indonesian Agency for Meteorological, Climatological and Geophysics

*Corresponding Author, Received: 05 April 2026, Revised: 21 May 2026, Accepted: 29 May 2026

ABSTRACT: Settlement control is a critical design consideration for large-diameter oil tank ringwall foundations constructed on granular soils, where stress-dependent stiffness and spatial variability can significantly influence serviceability performance. This study aims to the settlement behavior of stone-column-reinforced dense sand and compares a nonlinear power-law settlement model against a conventional linear baseline using plate load test (PLT) data. Laboratory-scale PLTs were conducted on dense sand (Dr = 80%) with configurations of untreated soil and sand reinforced with one to three stone columns. The results show that stone column inclusion significantly reduces settlement, with values decreasing from 21.3 mm in untreated sand to 9.87 mm, 6.42 mm, and 5.19 mm for one, two, and three-column configurations. The settlement reduction ratios reached approximately 76%, with diminishing incremental improvement as column number increased. The power-law model outperformed the linear baseline, achieving coefficients of determination (R^2) of 0.986-0.995 compared to 0.728-0.936, and substantially lower prediction errors across all configurations, a power-law formulation thus provides a better fit to the observed data than a linear assumption.

Keywords: Stone columns; Settlement behavior; Nonlinear modeling; Plate load test; Power-law model

1. INTRODUCTION

Large-diameter oil storage tanks are commonly supported by ringwall foundations to control bearing pressure while limiting differential settlement and tilt. In this foundation type, applied stresses are distributed over a wide radial footprint. Consequently, even moderate spatial variability in near-surface stiffness can lead to circumferential settlement gradients that may affect the tank shell and connected systems. Field evidence indicates that settlement and tilt often govern foundation design. For example, a 20 m high fuel tank supported on vibro-replacement stone columns satisfied a bearing demand of 200 kPa, while maintaining maximum settlement below 50 mm and tilt below 10 mm, provided that construction quality effectively controlled ground variability [1].

In granular soils, settlement is primarily governed by stress-driven particle rearrangement and shear strain mobilization, resulting in stiffness that depends on both density and stress level. This contrasts with simplified linear settlement assumptions often adopted for saturated fine-grained soils, where constant compressibility may be adequate over limited stress ranges. In sands, however, plate load test results typically exhibit nonlinear (curved) load-settlement responses, reflecting stress-dependent stiffness and progressive plasticity. This distinction has important implications for ringwall serviceability assessment, as neglecting such nonlinearity may lead to biased settlement predictions and misleading configuration comparisons.

Stone columns (including vibro-replacement columns) are widely used as a ground improvement technique because they enhance composite stiffness, mobilize higher shear resistance through soil–column interaction, and provide lateral confinement. In saturated conditions, they also facilitate drainage and accelerate pore pressure dissipation. Previous studies have demonstrated their applicability in soft soils, collapsible deposits, and liquefaction-prone sands, including the beneficial effects of geosynthetic encasement in weak surrounding soils [2–5].

Despite the extensive body of research on stone columns, several methodological limitations restrict their direct applicability to ringwall serviceability in granular soils. First, many settlement models assume linear stiffness behavior, which is inconsistent with stress-dependent sand response. Second, a large portion of experimental and numerical studies focuses on soft clays, where consolidation and drainage govern behavior [6,7]. Third, many studies emphasize liquefaction performance or cyclic response, whereas service-level static settlement remains less explored, despite its importance for operational conditions [8–10].

A widely adopted framework for analyzing stone column behavior is the unit-cell concept, in which a single column and its tributary soil are treated as an axisymmetric composite system. This approach enables the evaluation of stress sharing and stiffness contrast between the column and the surrounding soil. Experimental studies have shown that stress concentration can be significant and depends on several key parameters, which reinforces the need for models that explicitly consider composite behavior rather than assuming homogeneous ground conditions [11]. However, a research gap remains in developing performance-based settlement models that are consistent with sand behavior and are directly calibrated using controlled plate load test data.

Ground improvement for granular soils under service loading remains underserved by the existing literature on stone columns, which is dominated by soft-clay consolidation and liquefaction-mitigation studies. This study develops a configuration-specific settlement model for stone-column-reinforced dense sand under plate loading, calibrated directly from experimental data and supported by quantitative model comparison. The results are intended to guide the selection of modeling approaches for serviceability assessment of ringwall foundations, with the recognition that laboratory findings require further site-specific validation before field application.

Accordingly, this study aims to (i) quantify the settlement reduction achieved by one to three stone columns installed in dense sand (Dr = 80%), and (ii) develop and compare a nonlinear power-law settlement model against a linear baseline, with both models calibrated using plate load test data and evaluated using standard goodness-of-fit metrics. While nonlinear load-settlement formulations for granular media are established in principle, the specific contribution of this study is the systematic calibration and comparison of a power-law model under finite-plate laboratory conditions for stone-column-reinforced dense sand, coupled with a unit-cell stress-sharing framework. The results provide a basis for evaluating reinforcement configurations and for guiding the selection of serviceability-level settlement models in the design of ringwall foundations, subject to further field-scale validation. The remainder of this paper is organized as follows: Section 2 material and methods; Section 3 describes the settlement modeling framework and discusses experimental results and model performance; and Section 4 summarizes the main conclusions.

2. RESEARCH SIGNIFICANCE

This study provides an empirical contribution to understanding how dense sand and stone column reinforcement influence deformation behavior and bearing performance under ringwall foundation loading conditions. Through controlled plate load tests on uniformly graded sand prepared at a relative density of 80%, the study produces calibrated experimental data that can serve as a reference for further development and validation of numerical models for reinforced granular ground. The proposed power-law interpretation also offers a practical basis for linking laboratory testing, field plate load tests, and numerical simulation in evaluating settlement performance, while requiring site-specific validation before field application.

3. MATERIAL AND METHODS

3.1 Soil Characterization

3.1.1 In-situ investigation

Preliminary site investigation was conducted using cone penetration tests (CPT) and standard penetration tests (SPT) to establish the stratigraphy and density profile of the representative sand deposit. CPT soundings (10 locations) reached depths of approximately 10.8-21.8 m, while SPT borings (5 locations) extended to 21.15-23.15 m, terminating at refusal or target depth.

The subsurface profile consisted predominantly of sand with a fines content of approximately 10-20%, classified as poorly graded to silty sand (SP-SM). Cone resistance and SPT N-values ranging from 15 to 35 indicate medium to dense sand conditions. These field observations guided the selection of representative laboratory sand and the target relative density adopted in the tests.

3.1.2 Laboratory testing and soil properties

Laboratory grain-size distribution analysis confirmed that the material used for the model ground was predominantly sand. The composition consisted of 3.16% gravel, 94.53% sand, 0.59% silt, and 1.71% clay, consistent with a poorly graded sand (SP) classification with a uniformity coefficient Cu ≈ 2.38. The dry unit weight ranged from approximately 14.6 kN/m³ in the loose state to 17.65 kN/m³ at Dr = 80%, representing dense sand conditions. Direct shear tests yielded an internal friction angle ϕ ≈ 35°, indicating predominantly frictional behavior.

The laboratory sand was selected to represent the granular of the field deposit while controlling for the confounding effects of fines on permeability, compressibility, and column-soil interaction. The laboratory material has a fines content below 2.3%, compared to 10-20% in the field deposit (SP-SM). This divergence was intentional the clean sand provides a controlled lower-bound reference in which stress-dependent particle rearrangement, rather than fines-dominated compressibility or partial drainage, governs the load-settlement response. The presence of additional fines in the field material would generally increase compressibility at low stress levels and may alter the power-law exponent β. The present laboratory dataset therefore represents a controlled granular reference direct extrapolation to the site-specific soil with higher fines content requires additional testing of the representative gradation.

3.2 Experimental Setup

A rigid test box was used to prepare a controlled sand bed for the installation of laboratory-scale stone columns. Sand was placed in thick layers of 0.10 m to achieve a total specimen height of 1.0 m. The target relative density (Dr = 80%) was achieved using a mass-controlled placement method based on the required unit weight and layer volume. Compaction procedures were applied consistently for each layer to minimize spatial variability in stiffness.

The experimental setup consisted of a rigid test tank, loading system, and instrumentation arranged to perform plate load tests on both untreated and reinforced sand. A schematic view of the setup is shown in Figure 1. The test tank had plan dimensions of approximately 1.2 m × 1.2 m and a height of 1.21 m. The ratio of tank plan dimension to plate diameter is approximately 4.8 (1.2 m / 0.25 m), which exceeds the minimum ratio of 4 commonly cited in model test practice and is consistent with values adopted in comparable laboratory studies [22,16]. Nevertheless, the rigid tank walls impose passive lateral confinement that does not replicate field conditions where lateral displacement of surrounding sand is unconstrained. This may result in a slight overestimate of composite stiffness relative to open-field conditions. Because all four configurations were tested in the same rigid tank under identical boundary conditions, this effect is systematic and consistent across configurations; comparative trends such as settlement reduction ratios and stiffness gains are therefore not materially affected, though absolute settlement magnitudes should be interpreted with this constraint in mind.

Vertical loads were applied using a mechanical jack mounted on a loading frame and transferred to the soil through a rigid circular steel plate with a diameter of 0.25 m (area Ap ≈ 0.0491 m²). The applied load was measured using a proving ring (factory-calibrated, calibration conducted within 12 months of testing), and settlement was recorded using a dial gauge with a resolution of 0.01 mm, calibrated against a reference micrometer prior to each test series.

No anti-friction treatment was applied to the interior surfaces of the rigid steel tank. Wall friction, if mobilized, would tend to resist downward movement of the sand mass, potentially reducing measured settlement slightly relative to a frictionless boundary. Because this condition is identical across all four configurations, it does not affect comparative results between reinforced and unreinforced cases. To verify that the target relative density (Dr = 80%) was achieved consistently throughout the specimen, the as-placed dry unit weight was checked by extracting thin-walled cylindrical sampling rings (inner diameter 50 mm, height 50 mm) from three locations distributed across the specimen (centre, mid-radius, and near the tank wall) following preparation of each 100 mm layer. Measured dry unit weights were within ± 0.2 kN/m³ of the target value of 17.65 kN/m³, corresponding to Dr = 80% ± 4%. Layers falling outside this tolerance were removed and recompacted.

All tests were conducted on air-dry sand (gravimetric water content w < 0.5% as measured prior to each test), under fully drained, unsaturated conditions. Pore pressure development was not expected and was not monitored. This condition is representative of granular fill above the groundwater table and simplifies interpretation of the load–settlement response as a purely mechanical, stress-dependent phenomenon without hydraulic coupling.

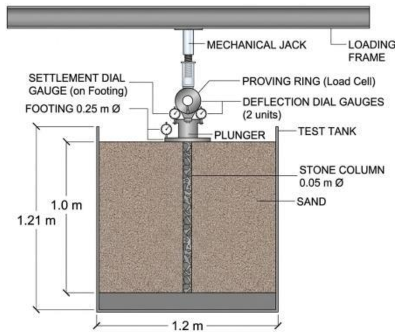

Fig. 1 Illustration of the experimental setup for plate load testing on stone-column-reinforced sand

3.3 Stone Column Configuration

Stone columns were constructed at laboratory scale with a diameter of 50 mm and a length of 1.0 m. The columns were arranged in a triangular pattern with a centre-to-centre spacing of 150 mm. Crushed aggregate was used as the column material, with representative particle sizes of 9.51 mm, 4.75 mm, and 2.36 mm. Stone columns were formed by driving a temporary casing (50 mm inner diameter) to full depth, filling with crushed aggregate in 100 mm sub-layers (each tamped with 10 blows of a 0.5 kg rod), and then withdrawing the casing. This replacement method displaces some surrounding sand; the effect on local density was not independently quantified in the present study and is acknowledged as a limitation.

Four test configurations were considered: untreated sand (no stone column) and reinforced sand with one, two, and three stone columns located within the loading plate footprint (Figure 2). The area replacement ratio (A_c) are defined in Equation 1-3 for a triangular pattern is defined as:

$$A_{\text{cell}} = \frac{\sqrt{3}}{2} s^2 \quad (1)$$

$$A_c = \frac{\pi D_c^2}{4} \quad (2)$$

$$a_r = \frac{A_c}{A_{\text{cell}}} \quad (3)$$

where s = 0.150 m is the column spacing, D_c = 0.050 m is the column diameter, A_{cell} = 0.01949 m², A_c = 0.001963 m², and ar ≈ 0.101 (approximately 10.1%). For multiple-column configurations under a finite loading plate, an effective replacement ratio ($a_{r,eff}$) may be defined based on the total column area within the plate footprint. The $a_{r,eff}$ values are approximately 4.0%, 8.0%, and 12.0% for one, two, and three columns, respectively [11-17].

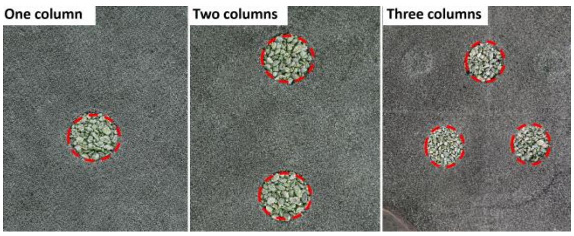

Fig. 2 Stone column configuration and layout relative to the loading plate

3.4 Plate Load Test (PLT) Configuration and Procedure

3.4.1 Plate geometry and instrumentation

Plate load tests (PLTs) were conducted using a rigid circular steel plate with a diameter of 0.25 m, corresponding to an area of approximately 0.0491 m². Settlement was measured using a dial gauge with a resolution of 0.01 mm. Vertical loads were applied incrementally using a controlled loading system. The applied load was determined from the target stress and plate area using the standard stress–area relationship:

where *P* is the applied load, *q* is the applied stress, and A_p is the plate area.

$$\mathrm{P} = \mathrm{q}A_p \quad (4)$$

3.4.2 Loading procedure

The loading program consisted of incremental stress application over a range of approximately 62.5-437.5 kPa. Each load increment was maintained until the corresponding settlement response was recorded.

The tests included both loading and unloading phases and residual settlement behavior. This approach allows assessment of irreversible deformation associated with particle rearrangement and plasticity in sand. Such behavior is relevant for ringwall foundations, where operational conditions may involve staged loading and unloading cycles [18].

3.4.3 Repeatability and experimental uncertainty

To assess test-to-test variability, each configuration was subjected to sequential replicate tests using a convergence criterion. For the untreated sand, one and two-column configurations, two replicate tests were conducted per configuration. For the three-column configuration, three replicates were performed. In each case, the second test was compared against the first, if the maximum settlement at peak applied stress differed by less than 10% between consecutive replicates, the configuration was considered reproducible and testing was stopped. If the difference exceeded this threshold, an additional replication was conducted. This criterion was met within two tests for the untreated, one, and two-column cases, and within three tests for the three-column case.

The reported load-settlement curves represent the mean response across the accepted replicates for each configuration. Test-to-test differences in maximum settlement remained below 10% across all configurations, indicating acceptable reproducibility under the controlled density preparation protocol. Because the number of replicates per configuration is small (two to three), formal confidence intervals on settlement reduction ratios and fitted model parameters cannot be established with high statistical precision. The reported values should therefore be interpreted as indicative of trends and relative performance between configurations, with the acknowledgement that a larger replicate set would be required to formally quantify parameter uncertainty.

3.4.4 Data reduction outputs

The primary output of each PLT was the load–settlement curve. To quantify the improvement effect of stone columns, the settlement reduction ratio (SRR) was defined as:

$$SRR = \left(1 - \frac{S_{SC}}{S_0}\right) \times 100\% \quad (5)$$

where S_0 is the settlement of untreated sand and S_{SC} is the settlement of the reinforced case at the same reference stress.

To evaluate serviceability stiffness, the modulus of subgrade reaction (K_s) was determined from the load-settlement response using a secant definition:

$$K_s = \frac{q}{s} \quad (6)$$

$$K_s = \frac{\Delta q}{\Delta s} \quad (7)$$

K_s is indicator for comparing stiffness improvement across different configurations. Similar interpretations of stiffness and stress sharing have been reported in unit-cell and consolidation-based studies [11,17].

3.5 Settlement Modeling and Evaluation

3.5.1 Linear baseline model

A linear settlement model was adopted as a baseline, in which settlement is assumed to be proportional to applied stress:

$$\mathrm{s} = \alpha q \quad (8)$$

where α (mm/kPa) is a regression parameter. This formulation implicitly assumes constant stiffness over the applied stress range and is commonly used in simplified serviceability analyses.

3.5.2 Nonlinear power-law model

To account for the stress-dependent behavior of dense sand, a nonlinear power-law settlement model is derived from first principles by combining the unit-cell stress-sharing concept with a stress-dependent compressibility relationship for granular materials.

Unit-cell stress sharing, following Kumar & Samanta (2020) [11], the total applied stress σ is partitioned between the stone column (σsc) and the surrounding sand (σs) using the area replacement ratio ar and stress concentration ratio n = σsc / σs:

$$a = \frac{A_{sc}}{A} \quad (9)$$

$$\sigma = a\,\sigma_{sc} + (1 - a)\,\sigma_s \quad (10)$$

$$\sigma_s = \frac{\sigma}{(1 - a) + an}, \sigma_{sc} = \frac{n\,\sigma}{(1 - a) + an} \quad (11)$$

where ar is the area replacement ratio, dimensionless ≈ 0.101 for the present configuration, n is the stress concentration ratio (dimensionless, typically 3-6 for dense granular soils [11]), σs is the stress acting on the surrounding sand (kPa), and σsc is the stress acting on the stone column (kPa).

Stress-dependent compressibility of sand. For dense sand, the constrained modulus M increases with stress level following a power-law relationship analogous to the Janbu tangent modulus framework:

$$M(\sigma_s) = M_0 \left(\frac{\sigma_s}{p_a}\right)^{\lambda} \quad (12)$$

where M_0 (kPa) is a reference constrained modulus, p_a = 100 kPa is atmospheric pressure used as a reference stress, and λ (dimensionless, 0 < λ < 1) is a stiffness exponent characterizing the stress-dependency of sand compressibility.

Integration to yield the power-law settlement model. The incremental settlement of the sand layer of effective thickness H beneath the plate under stress increment dσs is:

$$d_s = \left(\frac{\sigma_s}{M(\sigma_s)}\right) H\, d\sigma_s \quad (13)$$

Substituting Equation (12) into (13) and integrating over the applied stress range, while substituting the stress-sharing relationship of Equation (11), yields a settlement expression of the form:

$$s(\sigma) = K\,\sigma^{\beta} \quad (14)$$

where K (mm·kPa$^{-\beta}$) and β (dimensionless) are composite model parameters that absorb the effects of the area replacement ratio, stress concentration ratio, reference modulus M_0, and stiffness exponent λ. This formulation is equivalent to Equation (8) rewritten with physically grounded parameters, K encodes the composite stiffness of the reinforced ground at unit stress, and β characterizes the degree of stress-dependent nonlinearity. All symbols are defined in the Notation section before the References. Similar nonlinear approaches have been applied in the analysis of granular column systems [19, 20].

3.5.3 Model evaluation metrics

Model parameters (α for the linear model, K and β for the power-law model) were obtained through nonlinear least-squares regression of the experimental load-settlement data. Model performance was evaluated using three complementary metrics: the coefficient of determination (R^2), root mean square error (RMSE, mm), and the Akaike Information Criterion (AIC). The ΔAIC column in Table 1 reports the difference AIC_{linear}-$AIC_{power\text{-}law}$, positive values indicate that the power-law model is favored. These metrics allow comparison between models with different numbers of parameters while accounting for goodness-of-fit and parsimony.

4. RESULTS AND DISCUSSION

4.1 Load-Settlement Behavior

Figure 3 presents the measured load-settlement response under vertical loading and unloading for untreated sand and the reinforced configurations. Across the entire stress range, the inclusion of stone columns significantly reduced settlement and increased the apparent stiffness of the composite ground.

At the maximum applied stress, the untreated sand exhibited a settlement of approximately 21.3 mm. The installation of a single stone column reduced the settlement to approximately 9.87 mm, while two and three columns further reduced it to approximately 6.42 mm and 5.19 mm, respectively. The most substantial improvement occurs when transitioning from untreated to reinforced conditions, whereas additional columns provide progressively smaller reductions in settlement. The observed trends are consistent with previous studies reporting reduced settlement and increased stiffness with increasing column number [21,22].

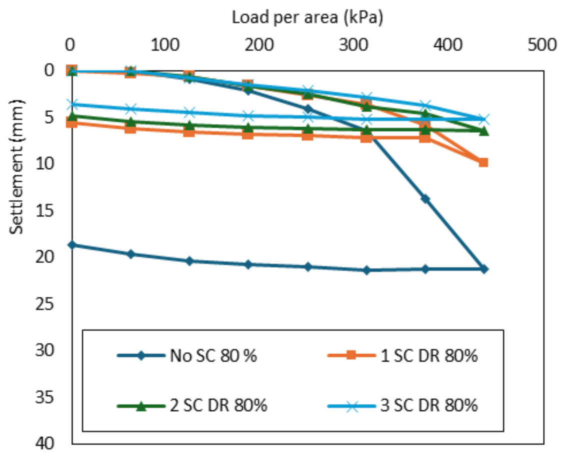

Fig. 3 Load–settlement response of untreated and stone-column-reinforced sand under vertical loading and unloading

4.2 Performance Metrics and Stiffness Evaluation

The improvement in settlement performance was quantified using the settlement reduction ratio (SRR) at the maximum applied stress. The SRR values were approximately 54% for one column, 70% for two columns, and 76% for three columns, confirming a clear enhancement with increasing number of columns.

The diminishing incremental improvement from two to three columns can be understood through the geometry of stress distribution beneath the loading plate. The effective area replacement ratio under the 0.25 m plate increases from $a_{r,eff} \approx 4\%$ (one column) to 8% (two columns) to 12% (three columns), with a constant incremental increase of 4.0 percentage points per column. However, settlement reduction does not scale linearly with $a_{r,eff}$ because (i) the column directly beneath the plate centre carries the highest proportion of applied load; (ii) additional columns placed at triangular-pattern offsets (spacing 0.15 m ≈ 0.6 × plate diameter) fall progressively closer to the perimeter of the stress bulb, where vertical stress intensity is lower; and (iii) as the stress bulb depth beneath the 0.25 m plate at the maximum applied stress is approximately 0.25-0.30 m, the lower portions of the 1.0 m columns lie in a low-stress zone and contribute less to settlement reduction than their geometric presence would suggest. As column influence zones begin to overlap, the composite system approaches a limiting stiffness, and further columns provide diminishing incremental improvement. Similar geometric saturation effects have been reported in previous studies [16,17].

The settlement improvement is attributable to three interacting mechanisms, approximately ranked by their relative importance for the present configuration (i) direct load transfer to the stiffer column material (dominant mechanism), where the unit-cell stress-sharing diverts a disproportionate fraction of the applied load to the column, reducing the stress on the compressible sand matrix, the stress concentration ratio n estimated for this configuration is approximately 3-5, consistent with the range reported by Kumar & Samanta (2020) [11]; (ii) lateral confinement of the surrounding sand (secondary mechanism), where the stone column suppresses lateral strain in the adjacent sand, increasing the effective constrained modulus; (iii) installation densification, which is minor in the laboratory casing-extraction method used here compared to field vibro-replacement.

The modulus of subgrade reaction (Ks) increased consistently with column number, reflecting enhanced load sharing where a greater portion of applied stress is transferred to the stiffer column material. The unloading-reloading response shown in Figure 3 reveals residual settlements in all configurations, indicating that irreversible deformation from particle rearrangement and localized shear strain occurs even within the applied stress range. This behavior highlights a fundamental limitation of linear stiffness assumptions: a constant modulus cannot represent the path-dependent response of granular materials. It should be noted that SRR and Ks are configuration-dependent indicators and should be interpreted in a relative sense rather than as absolute design parameters.

4.3 Development and Validation of Settlement Model

Both linear and power-law formulations were fitted to the experimental load-settlement data for each configuration. The goodness-of-fit results (Table 1) indicate that the power-law model consistently outperforms the linear model, with R^2 = 0.986-0.995 compared to 0.73-0.94 for the linear model, and substantially lower RMSE values across all cases.

Table 1. Model fit comparison: linear vs power-law

Test	Linear R^2	Linear RMSE (mm)	Power-law R^2	Power-law RMSE (mm)	AIC (Linear-New)
Untreated sand (Dr 80%)	0.728	3.726	0.995	0.517	29.61
1 column (Dr 80%)	0.797	1.422	0.986	0.376	19.29
2 columns (Dr 80%)	0.916	0.634	0.995	0.159	20.09
3 columns (Dr 80%)	0.936	0.434	0.994	0.137	16.50

The improvement is particularly evident for untreated sand, where RMSE decreases from 3.73 mm to 0.52 mm. The positive ΔAIC values across all configurations confirm that the improved fit reflects a more appropriate functional form rather than merely the addition of a model parameter. As shown in Figures 4-7, the linear model exhibits systematic deviation at higher stress levels, whereas the power-law model closely follows the curvature of the experimental response.

A notable trend is the reduction in the nonlinearity exponent β from approximately 3.09 for untreated sand to 1.56 for the three-column configuration.

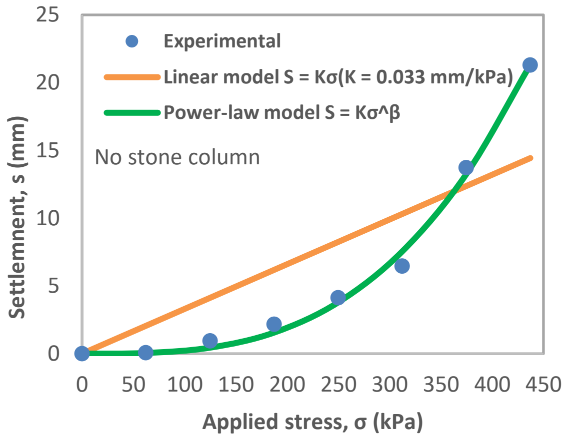

Fig. 4 Model fit comparison between linear and power-law formulations for untreated sand

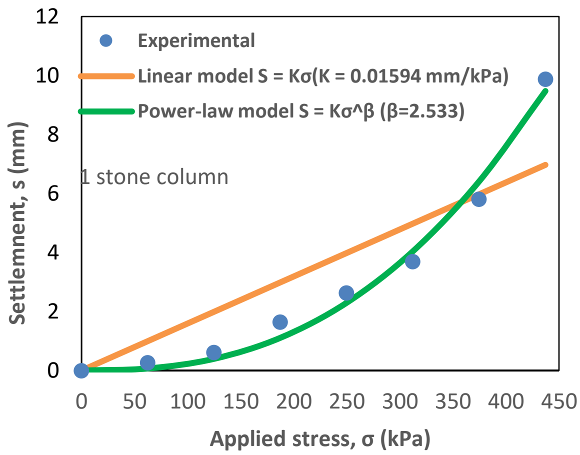

Fig. 5 Model fit comparison between linear and power-law formulations for the one-column configuration

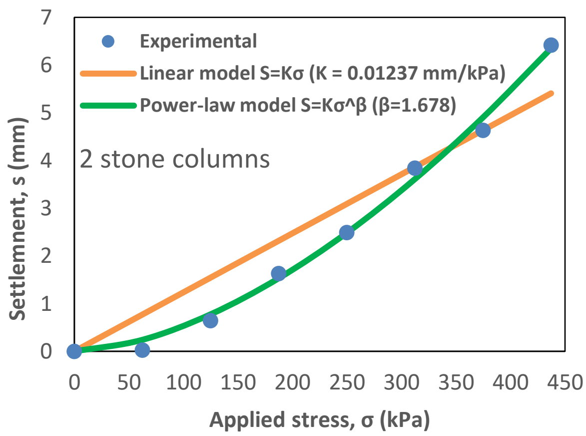

Fig. 6 Model fit comparison between linear and power-law formulations for the two-column configuration

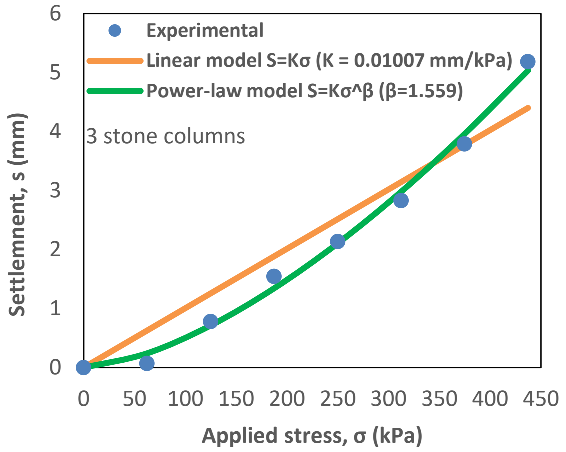

Fig. 7 Model fit comparison between linear and power-law formulations for the three-column configuration

Physically, β captures the curvature of the load–settlement response: values significantly greater than 1.0 indicate strongly stress-dependent stiffness, where incremental stiffness degrades rapidly with increasing load, while values approaching 1.0 reflect nearly linear behavior. In untreated sand, large β reflects pronounced progressive shear strain mobilization and particle rearrangement that dominate compressibility at higher stress levels. As stone columns are added, load sharing transfers a greater portion of stress to the stiffer granular column material, reducing the net stress acting on the surrounding sand and thereby suppressing the nonlinear response. The systematic decrease in β with increasing column number is therefore a direct indicator of composite stiffening, not a statistical artifact, but a physically meaningful measure of how reinforcement shifts the governing deformation mechanism from stress-driven particle rearrangement toward a more constrained, column-controlled response. It should be noted that β is fitted against a small number of replicates per configuration, its robustness across different sand densities, column geometries, or loading sequences requires further experimentation.

Figure 8 presents the residuals for both models across all configurations. For untreated sand, the linear model exhibits a pronounced systematic pattern, negative residuals at intermediate stress levels and large positive residuals at higher stresses indicating a fundamental mismatch in the assumed functional form. The power-law model produces smaller, more evenly distributed residuals. For reinforced cases, residual magnitudes decrease for both models, consistent with the more stable, less nonlinear composite response. The linear model, however, retains noticeable bias at higher stress levels even in reinforced configurations, whereas the power-law model maintains small, randomly distributed residuals throughout [23].

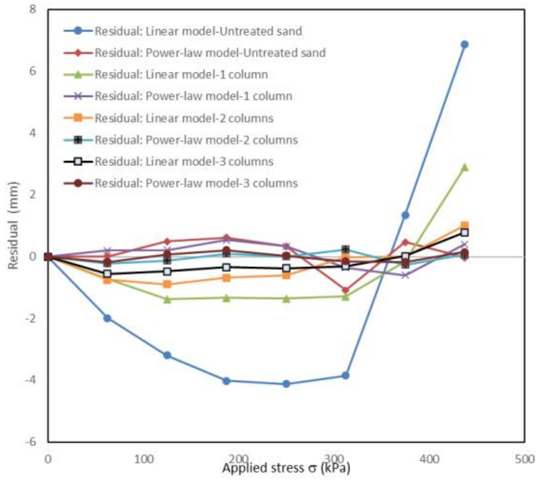

Fig. 8 Residuals between measured and predicted settlement for linear and power-law models under different stone column configurations

The present study focuses on dense sand (Dr = 80%) reinforced with one to three stone columns under static plate loading, and the limitations of the current study must be explicitly acknowledged. First, the experimental setup involves a rigid test tank (1.2 m × 1.21 m) with a 0.25 m diameter loading plate, yielding a tank-to-plate width ratio of approximately 4.8. While adequate for comparative testing, the rigid boundary does not replicate field conditions. Second, tests were conducted under static, monotonic loading only; field ringwall foundations may experience staged construction loads and differential settlements that the current dataset cannot address. Third, the model is fitted and validated exclusively against a single laboratory dataset representing dense sand at Dr = 80%, the parameter space (density, column diameter, spacing, length, aggregate gradation) is narrow. Fourth, the laboratory material (fines content < 2.3%) differs from the field deposit (10-20% fines), as discussed in Section 2.1. Fifth, the number of replicates per configuration is small (two to three), and no formal confidence intervals on SRR or model parameters can be established.

The present study is interpreted as a controlled comparative investigation demonstrating the superiority of power-law over linear settlement modeling for dense, stone-column-reinforced sand under plate loading. Extension to field scale requires independent validation against site-specific in-situ data, including CPTu or SDMT-derived stiffness profiles, and calibration of scale factors that account for stress-path differences between small-scale plate loading and large-diameter foundation behavior. Further validation under varying density states, column geometries, and loading conditions is necessary before the framework can be applied with confidence in practice [24-27].

The implications for ringwall foundation design are twofold. First, performance is highly sensitive to differential settlement; ground improvement strategies must therefore aim to reduce both total settlement and spatial variability. Second, the proposed modeling framework provides a practical basis for calibration using site-specific plate load tests and in-situ stiffness indicators such as CPTu, SDMT, or geophysical methods [12-15], enabling a consistent linkage between laboratory observations and field-scale performance.

5. CONCLUSION

This study investigated the settlement behavior of stone-column-reinforced dense sand under plate load testing and compared a power-law settlement model against a linear baseline, with both fitted to the experimental load-settlement data. The following conclusions are drawn within the scope of this study: Stone column inclusion significantly reduces settlement. Maximum settlement decreased from approximately 21.3 mm for untreated sand to 9.87 mm, 6.42 mm, and 5.19 mm for one, two, and three-column configurations, respectively, at the maximum applied stress of 437.5 kPa.

Settlement reduction ratios reached approximately 54%, 70%, and 76% for one, two, and three columns, respectively. The diminishing incremental improvement with additional columns is explained by geometric saturation of the stress bulb beneath the loading plate and overlapping column influence zones, consistent with a unit-cell geometric argument.

The power-law model provides a substantially improved representation of settlement behavior, with R^2 = 0.986-0.995 compared to 0.73-0.94 for the linear model, and significantly lower RMSE across all configurations. The AIC confirms that the improvement reflects a more appropriate functional form rather than increased model complexity.

The nonlinearity exponent β decreases from approximately 3.09 for untreated sand to 1.56 for the three-column configuration, providing a physically meaningful indicator of composite stiffening as reinforcement increases. The proposed model is calibrated for dense sand (Dr = 80%) under controlled laboratory plate loading and should not be applied directly to field design without recalibration. A single relative density, one column geometry, static loading only, a finite rigid test tank, and the absence of site-representative fines content in the laboratory material. Subject to these constraints, the model provides a reproducible and statistically supported calibration reference for serviceability assessment of stone-column-reinforced granular soils, and the calibration procedure described is transferable to field-scale plate load tests and in-situ stiffness measurements.

6. ACKNOWLEDGEMENTS

The authors acknowledge the support of the Department of Civil and Environmental Engineering, Faculty of Engineering, Universitas Gadjah Mada, in providing laboratory facilities for this research. The authors also thank Yuli Fajarwati in conducting the proofreading the manuscript.

7. REFERENCES

1. Jamsawang P., Bergado, D. T., Voottipruex, P., Baez, F., and Jongpradist, P., A Case Study of the Application of Wet Top-Feed Vibro Replacement Stone Columns as Foundation Supports for a Fuel Tank in a Reclamation Area, Bull Eng Geol Environ, 84(1), 2024, p. 4. https://doi.org/10.1007/s10064-024-04027-8.
2. Abhishek S. V., Rajyalakshmi, K., and Madhav, M. R., Engineering of Ground with Granular Piles: A Critical Review, International Journal of Geotechnical Engineering, 10(4), 2016, pp. 337–357. https://doi.org/10.1080/19386362.2016.1145942.
3. Suriya P., Subathra, P., Gopiprasath, P., and Lakshminarayana, V., Stabilization of Soft Soil Using Stone Column – The Review, 2017.
4. Das M., and Das A. K., Performance of Reinforced Stone Column: A Comprehensive Review, European Journal of Environmental and Civil Engineering, 28(15), 2024, pp. 3587–3616. https://doi.org/10.1080/19648189.2024.2356007.
5. Jayarajan J. and Karpurapu R., Encased Columnar Inclusions in Soft Grounds - A Review, 49(1), 2018, pp. 106–118.

6. Hataf N., Nabipour, N., and Sadr, A., Experimental and Numerical Study on the Bearing Capacity of Encased Stone Columns, Geo-Engineering, 11(1), 2020, p. 4. https://doi.org/10.1186/s40703-020-00111-6.
7. Abdelhamid M., Ali, N., and Abdelaziz, T., Experimental Study on the Behavior of Floating Encased Stone Columns in Collapsible Soils, Indian Geotech J, 56(3), 2026, pp. 1423–1444. https://doi.org/10.1007/s40098-025-01189-4.
8. Ellouze S., Bouassida, M., Ben Salem, Z., and Znaidi, M. N., Numerical Analysis of the Installation Effects on the Behavior of Soft Clay Improved by Stone Columns, Geomechanics and Geoengineering: An International Journal, 2016. https://doi.org/10.1080/17486025.2016.1164903.
9. BenSalem Z., Frikha, W., and Bouassida, M., Liquefaction Potential of Reinforced Soil by Stone Columns, Geomechanics and Geoengineering, 19(6), 2024, pp. 915–932. https://doi.org/10.1080/17486025.2024.2330564.
10. Wani K. M. N. S., Ahmad, N., Kashani, S. N. F., Muzafar, Z., Gul, N., and Kumar, R., Advancements in Liquefaction Mitigation Techniques for Soil Improvement: A Comprehensive Review, Int. J. Pavement Res. Technol, 2025, https://doi.org/10.1007/s42947-025-00649-7.
11. Kumar G. and Samanta M., 2020, “Experimental Evaluation of Stress Concentration Ratio of Soft Soil Reinforced with Stone Column,” Innov. Infrastruct. Solut., 5(1), p. 18. https://doi.org/10.1007/s41062-020-0264-6.
12. Amoroso S., Rollins, K. M., Monaco, P., Holtrigter, M., and Thorp, A., Monitoring Ground Improvement Using the Seismic Dilatometer in Christchurch, New Zealand, Geotech. Test. J., 41(5), 2018, pp. 946–966. https://doi.org/10.1520/GTJ20170376.
13. Amoroso S., García Martínez, M. F., Monaco, P., Tonni, L., Gottardi, G., Rollins, K. M., Minarelli, L., Marchetti, D., and Wissmann, K. J., Comparative Study of CPTU and SDMT in Liquefaction-Prone Silty Sands with Ground Improvement, Journal of Geotechnical and Geoenvironmental Engineering, 148(6), 2022, p. 04022038. https://doi.org/10.1061/(ASCE)GT.1943-5606.0002801.
14. Saha A. and Dey A. K., Assessing Combined Analysis of Electrical Resistivity Tomography and Multichannel Analysis of Surface Waves for Ground Improvement Assessment near By-Pass Road, Silchar, Assam, Exploration Geophysics, 54(5), 2023, pp. 474–492. https://doi.org/10.1080/08123985.2023.2168533.
15. Hartono N. and Fathani T. F., Design of stone column to mitigate soil liquefaction: cases study of Yogyakarta International Airport. Journal of the Civil Engineering Forum, 2023, https://doi.org/10.22146/jcef.5933.
16. Noorak A., Jamnongwong, M., and Rochanavibhata, U., The Study of Improved Silty Sand with Stone Columns under Consolidation Condition, Key Engineering Materials, 998, 2024, pp. 3–11. https://doi.org/10.4028/p-9kC9FA.
17. Rochanavibhata U., Noorak, A., Jongpradist, P., Makaratat, N., Jing, G., and Jamsawang, P., Consolidation Behavior of Silty Sand Improved by Stone Column, Transp. Infrastruct. Geotech., 12(1), 2024, p. 25. https://doi.org/10.1007/s40515-024-00470-y.
18. Kumar N. and Kumar R., Performance of Geosynthetic-Encased Stone Columns in Sandy Soils Subjected to Vertical Cyclic Loads, International Journal of Geomechanics, 25(1), 2025, p. 04024323. https://doi.org/10.1061/IJGNAI.GMENG-10283.
19. Sharma J. K. and Gupta P., Analysis and Settlement Evaluation of an End-Bearing Granular Pile with Non-Linear Deformation Modulus, SGEM, 40(3), 2018, pp. 188–201. https://doi.org/10.2478/sgem-2018-0022.
20. Yang G., Gao, J., Zhang, Y., and Feng, Q., Effects of Gravel Columns on Static and Dynamic Properties of Sand: A Laboratory Investigation, Sci Rep, 15(1), 2025, p. 41866. https://doi.org/10.1038/s41598-025-25868-7.
21. Chenari R. J., Fard, M. K., Chenari, M. J., and Sosahab, J. S., Physical and Numerical Modeling of Stone Column Behavior in Loose Sand, Int J Civ Eng, 17(2), 2019, pp. 231–244. https://doi.org/10.1007/s40999-017-0223-6.
22. Shahmandi A., Ghazavi, M., Barkhordari, K., and Hashemi, M., The Effect of Using Reinforced Granular Blanket and Single Stone Column on Improvement of Sandy Soil: Experimental Study, IJE, 36(8), 2023, pp. 1532–1547. https://doi.org/10.5829/IJE.2023.36.08B.13.
23. Singh I. and Sahu A. K., Multi-Blended Granular Columns Encased with Geosynthetics, Zeitschrift der Deutschen Gesellschaft für Geowissenschaften, 2024, pp. 73–88. https://doi.org/10.1127/zdgg/2024/0412.
24. Rezaei-Hosseinabadi M. J., Bayat, M., Nadi, B., and Rahimi, A., Sustainable Utilisation of Steel Slag as Granular Column for Ground

Improvement in Geotechnical Projects, Case Studies in Construction Materials, 17, 2022, p. e01333. https://doi.org/10.1016/j.cscm.2022.e01333.

25. Mahawish A., Bouazza, A., and Gates, W. P., Strengthening Crushed Coarse Aggregates Using Bio-Grouting, Geomechanics and Geoengineering, 14(1), 2019, pp. 59–70. https://doi.org/10.1080/17486025.2018.1521999.
26. Basack S., Siahaan, F., Indraratna, B., and Rujikiatkamjorn, C., Stone Column–Stabilized Soft-Soil Performance Influenced by Clogging and Lateral Deformation: Laboratory and Numerical Evaluation, International Journal of Geomechanics, 18(6), 2018, p. 04018058. https://doi.org/10.1061/(ASCE)GM.1943-5622.0001148.
27. Yazdandoust M. and Bastami, A., “Cyclic Behavior and Liquefaction Resistance of Loose Ground Improved by Granular Columns,” International Journal of Geomechanics, 24(11), 2024, p. 04024269. https://doi.org/10.1061/IJGNAI.GMENG-10171.